Kinetics and Mechanism of Selective Tungsten Deposition by LPCVD

Y. Pauleau* and Ph. Lami

Centre National d'Etudes des Télécommunications, 38243 Meylan, France

ABSTRACT

Tungsten films have been deposited selectively on oxide-patterned silicon wafers by the H_2 reduction of WF_6 in WF_6-H_2 and WF_6-H_2-Ar gas flow systems. The deposition rate of films was investigated as a function of reactant partial pressures. The reaction orders with respect to WF_6 and H_2 are zero and one-half, respectively. Under given experimental conditions, the growth rate of the selectively deposited W films was reduced by 32% when the deposition area increased by a factor of 10-100. This decrease in growth rate can be attributed to the effect of HF on the surface reaction. The selective nature of the process deteriorates with increasing deposition rate, WF_6 partial pressure, H_2 partial pressure, or deposition time. The loss of selectivity seems to be linked to an increase in HF partial pressure in the reactor.

Since the 1960's, the potential advantages of vapor-deposited tungsten as a metallization and interconnection material for silicon devices have become well-known (1). Tungsten is a promising candidate for contact and diffusion barriers, low resistance gates, and interconnect lines in VLSI circuits. W films have been prepared by chemical vapor deposition (CVD) in several gas systems (2). The hexafluoride vapor, WF_6, is currently used as a starting material. Under appropriate experimental conditions, W can be deposited selectively on oxide-patterned silicon wafers via the H_2 reduction of WF_6, *i.e.*, the metal can grow on monocrystalline and polycrystalline silicon surfaces while the surrounding oxide regions remain free of any deposit. Several etching and lithography steps are eliminated using the selective process to deposit tungsten on source, drain, and gate regions of MOS circuits. Owing to the advantages of selective deposition and the requirements for VLSI technology, the interest in vapor-deposited tungsten films has been revived (3, 4).

The growth rate of CVD tungsten metallurgical coatings by reduction of WF_6 with hydrogen has been investigated as a function of deposition temperature and reactant partial pressures (5, 6). Lately, the kinetics of W deposition has been examined at lower temperature-pressure combinations compatible with the selective process (7). The deposition rate dependence on the substrate temperature and the partial pressures of WF_6 and H_2 has been found consistent with the results obtained for deposition of tungsten metallurgical coatings. The selective nature of the W deposition process is dependent on various parameters such as deposition temperature, composition of WF_6-H_2 gas mixtures, and total pressure (8). However, the relationships between selectivity and processing parameters remain essentially qualitative.

The purpose of our experiments was to investigate the kinetics of W deposition via the H_2 reduction of WF_6 and the effect of H_2 and WF_6 partial pressures on selectivity. The metal was deposited on oxide-patterned silicon wafers in two stages. In a first step was grown a self-limiting layer of W via the Si reduction of WF_6 under fixed and constant experimental conditions. Then the growth of metallic films is continued via the H_2 reduction of WF_6 carried out under variable experimental conditions. The deposition rate of metal produced by the H_2 reduction of WF_6 and the selectivity of the deposition process have been determined as a function of the deposition parameters. The growth mechanism of tungsten films will be discussed in the following sections.

Experimental Procedure

The deposition of tungsten films was carried out in a low pressure CVD system with a three-zone resistance-heated horizontal furnace. This experimental setup is quite similar to systems described in previous papers (7-9). The reaction chamber was evacuated with a Roots blower backed by an oil rotary pump. To maintain the total pressure in the reactor constant, the pumping capacity of the vacuum system could be adjusted by introducing an argon stream at the entrance of the Roots blower. So, total pressure and gas flow could be varied independently of one on another. The temperature setting of the reactor was calibrated with an internal thermocouple, at the same pressure and gas flow as those used during the experiments. The temperature difference across the length of the boat was less than 1°C. The purities of WF_6, hydrogen, and argon gases were 99.8, 99.9995, and 99.9995%, respectively. The deposition process was controlled and monitored by a microprocessor.

20-40 Ω-cm p-type (100)-oriented single-crystal silicon wafers of 100 mm diam were used. These wafers were coated with a 40 nm thick thermal oxide layer. Then, a 800 nm thick undoped low temperature oxide (LTO) was deposited on top of the thermal oxide via LPCVD at 430°C. The test pattern for W selective deposition (Fig. 1) was delineated by standard photolithographic methods; the oxide layers were etched by dipping in a buffered HF solution. After photoresist stripping, a lot of 25 substrates was cleaned in a mixture of (2.5:1) H_2SO_4:H_2O_2 for 15 min, rinsed in deionized water, and nitrogen spin dried before storage in dust-proof containers. In the reactor, a quartz boat containing 80 wafers is positioned so that the substrate surface is parallel to the gas stream. The wafers are placed in eight rows (A to H) comprising five slots spaced 12 mm apart; two wafers are placed back to back in each slot. Only three or four wafers per deposition run were used as samples; the others were thermally oxidized dummy wafers. Prior to loading in the quartz boat, the test wafers were chemically etched to remove the native oxide layer on the bare silicon regions. This chemical treatment consisted of etching in a (10:1) HF solution for 20s, rinsing in deionized water, and a nitrogen spin dry.

Some W films were prepared via the Si reduction of WF_6. The substrate temperature was fixed at 285°C. The partial pressures of WF_6 and argon were 0.005 and 0.245 torr, respectively. The sheet resistance of films was determined as a function of the reaction time which varied between 2 and 12 min. This deposition process comprises several sequences. After loading the quartz boat into the furnace, which is at deposition temperature, the reactor is evacuated, purged with nitrogen at a pressure of 0.25 torr for 10 min, and again evacuated to a base pressure of 5×10^{-3} torr. The argon flow rate corresponding to the deposition conditions is established for 10 min to allow the substrate temperature to stabilize, and then WF_6 is introduced into the reactor for 2-12 min for W deposition on monocrystalline silicon.

The W deposition experiments via the H_2 reduction of WF_6 were carried out in two successive stages. The first stage consisted in the Si reduction of WF_6 performed under the experimental conditions described above. After this step, the reactor is purged with argon for 2 min, and the second stage of deposition via the H_2 reduction of WF_6 proceeds according to the following sequences. The ar-

*Electrochemical Society Active Member.

Downloaded on 2015-03-18 to IP 152.14.136.77 address. Redistribution subject to ECS terms of use (see ecsdl.org/site/terms_use) unless CC License in place (see abstract).

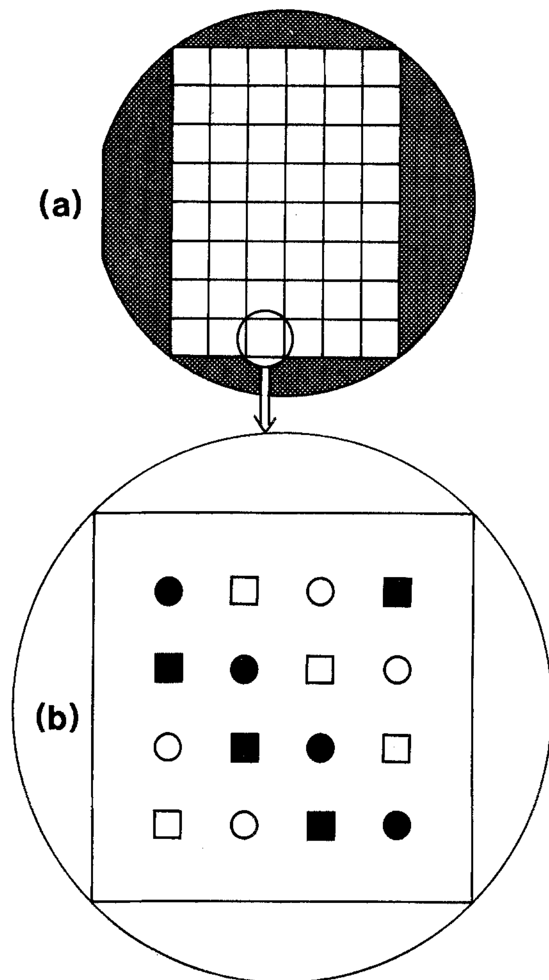

Fig. 1. a: Test pattern for selective deposition of tungsten on silicon wafers. Si (dark areas); SiO_2 (light areas). b: Magnification of 1 cm^2 of SiO_2 showing square windows of different sizes. Solid squares: 600 μm. Open squares: 400 μm. Solid circles: 200 μm. Open circles: 100 μm.

gon and hydrogen flow rates are established for 10 min, and then the deposition occurs when WF_6 is introduced into the reaction chamber. The deposition duration is fixed at 15 min. The gas flow rates and partial pressures of WF_6, hydrogen, and argon were varied as given in Table I. In all these experiments, the deposition temperature was maintained at 285°C since at this low temperature encroachment problems are suppressed (10) and excellent selectivity can be obtained (8).

The thickness of W films was measured using a stylus profilometer. Tungsten steps were etched in the large deposition zones near the wafer edges (Fig. 1). To delineate the steps, after coating with a protective wax layer, the samples were dipped in a $KOH(0.24M)$-$KH_2PO_4(0.25M)$-$K_3Fe(CN)_6(0.1M)$ solution for 1 min (2) after which the wax was stripped in trichlorethylene. The W deposition rate was derived from thickness measurements. To evaluate the selectivity of the process, the test wafers were observed by dark field optical microscopy at a magnification of 500. When a failure of selectivity occurred, minute shiny dots of tungsten could be detected on the oxide regions. Selectivity is less good at the edges of the large surfaces of deposition than in the center of samples. To characterize the quality of selectivity, different symbols are used in Fig. 3-5; the meaning of these symbols is shown in Table II.

Table I. Processing parameters for selective tungsten deposition at 285°C. (1 torr = 133 Pa)

	H_2	WF_6	Ar	Total
Flow rate (liter/min)	1-4	0.015-0.300	1-4	4-7
Pressure (mtorr)	180-1400	3-55	0-1200	250-1400

Table II. Symbols used to characterize the selective nature of the tungsten deposition process

△	Selective deposition
	Failure of Selectivity
▲	W dots on SiO_2 up to 1 mm from the edge of the large deposition zones.
◭	W dots on SiO_2 up to 10 mm from the edge of the large deposition zones.
▲	Non-selective deposition

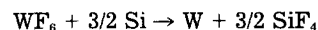

Results

Si reduction of WF_6.—The Si reduction of WF_6 proceeds according to the reaction (2, 9)

$$WF_6 + 3/2\ Si \rightarrow W + 3/2\ SiF_4$$

Tungsten films can form only on silicon regions, and this process is strictly selective. At 285°C and under the partial pressures of WF_6 and argon used, encroachment of W films along the SiO_2-Si interface does not occur. This result is consistent with that obtained by Moriya *et al.* (10). At the initial stage, the reaction of WF_6 with silicon is very fast. The sheet resistance of W films has been found to decrease very rapidly during the first 3 min; for reaction times longer than 3 min, the sheet resistance reaches a constant value (Fig. 2). The minimum resistivity is 30 $\mu\Omega$-cm, which is in good agreement with values reported in the literature (2). The metallic layers reach a limit in thickness once silicon is completely covered with a continuous, compact W layer. 15 nm thick W films were deposited during this step. The thickness of silicon consumed was about 30 nm. These thickness values deduced from scanning electron microscopic observations of samples are consistent with the data previously published (7, 9, 10).

H_2 reduction of WF_6.—When a WF_6-H_2 gas mixture is introduced into the reactor to deposit W on silicon, Si and H_2 react simultaneously with WF_6 (7, 10) and it is impossi-

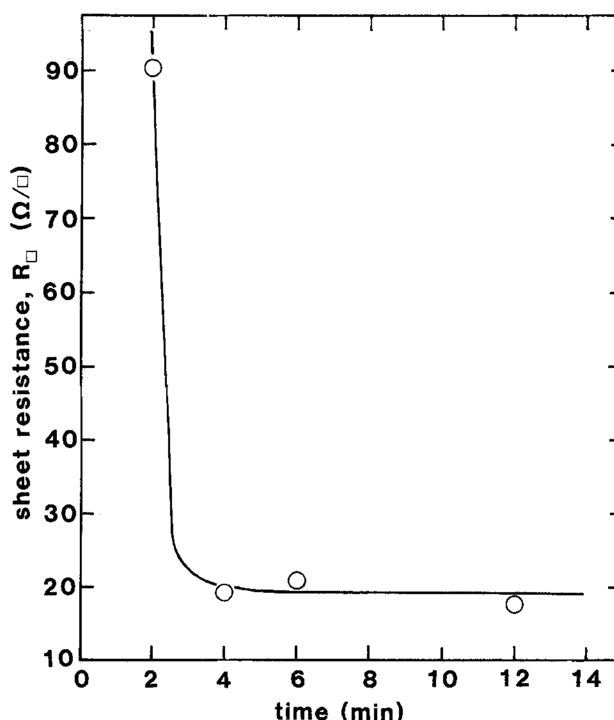

Fig. 2. Sheet resistance of W films vs. reaction time for films produced via the Si reduction of WF_6. Argon pressure = 0.245 torr; WF_6 pressure = 5 mtorr; deposition temperature = 285°C. (1 torr = 133 Pa.)

Downloaded on 2015-03-18 to IP 152.14.136.77 address. Redistribution subject to ECS terms of use (see ecsdl.org/site/terms_use) unless CC License in place (see abstract).

ble to determine accurately the thickness of W films grown via the H_2 reduction of WF_6 (2, 11)

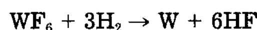

$$WF_6 + 3H_2 \rightarrow W + 6HF$$

To eliminate this uncertainty, a first deposition step consisting in the Si reduction of WF_6 was systematically carried out under the experimental conditions already described. W films prepared by the H_2 reduction of WF_6 were deposited on 15 nm thick tungsten layers formed during the first step. To determine the deposition rate, 15 nm of tungsten have been deducted from the total thickness of films obtained by α-step height measurements.

The growth rate of W films on wafers closest to the tube wall (positions 1 and 10 in rows A to H) was zero or very slight compared with the deposition rate on wafers placed within a row. Consequently, the results obtained on the outermost test wafers have been disregarded and only those found for wafers in an internal position (no. 2 to 9 in a row) are reported. The deposited material was determined to be polycrystalline W by x-ray diffraction techniques. In Fig. 3 is plotted the deposition rate of films produced from WF_6-H_2-Ar or WF_6-H_2 gas systems *vs.* WF_6 partial pressure. The hydrogen partial pressure was varied between 0.18 and 0.81 torr, and the argon partial pressure was adjusted to maintain a constant total pressure of 1.4 torr. The growth rate of W films is essentially independent of the WF_6 partial pressure with or without argon in the gas phase.

The deposition rate of W films prepared from WF_6-H_2-Ar gas mixtures under a constant total pressure of 1.4 torr was examined as a function of the H_2 partial pressure. During these experiments, the WF_6 partial pressure could be varied in a wide range (5-50 mtorr) without showing any effect on the deposition rate. The dependence of the growth rate on the H_2 partial pressure is shown in Fig. 4. The deposition rate of W films is proportional to the square root of H_2 partial pressure. The curve (C1) has been plotted using the kinetic data resulting from experiments carried out when the quartz tube, quartz boat, and dummy wafers were clean. Under these experimental conditions, the total surface area of W deposition was about 60 cm², *i.e.*, the deposition area was limited to the silicon area left exposed on the test wafers. The rate constant deduced from the slope of the straight line (C1) is equal to 8.12 nm-min^{-1}-torr$^{-1/2}$. With the processing parameters used, the quartz ware remains free of any W deposit during 20-25 runs; the cumulated thickness of metal deposited on silicon regions of the test wafers is between 1.5 and 2 μm. After about 25 runs, a W deposit could be detected on the quartz boat near the test wafer positions and on its downstream part. The quartz tube wall and some dummy wafers were also partially covered with a W deposit. The W layer formed progressively; nevertheless, it spread more and more rapidly during further runs.

Curve (Di) corresponds to kinetic data obtained for experiments performed with dirty quartz ware, *i.e.*, when a slight deposit of metal could be detected on the quartz

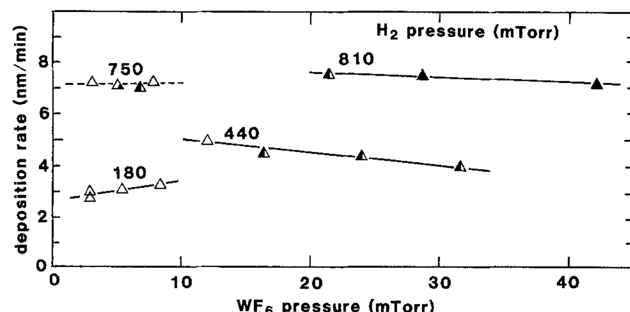

Fig. 3. Deposition rate *vs.* WF_6 partial pressure for W films deposited at 285°C from WF_6-H_2-Ar (solid line) or WF_6-H_2 (dotted line) gas systems. In WF_6-H_2-Ar mixtures, the total pressure was 1.4 torr; the H_2 partial pressures were 180, 440, and 810 mtorr. (1 torr = 133 Pa.) The meanings of symbols used for data points are given in Table II.

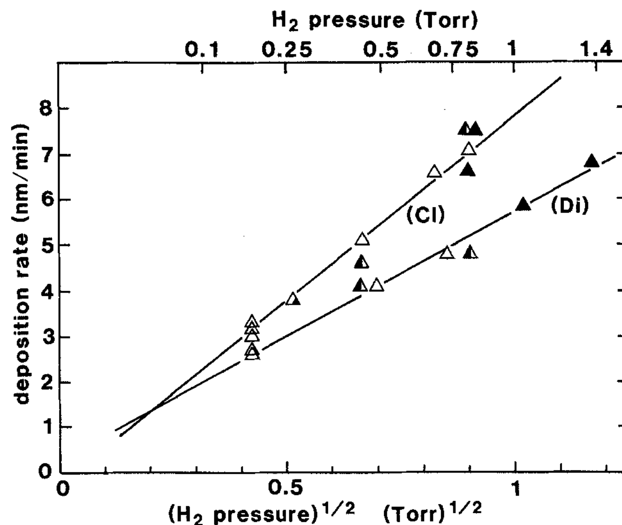

Fig. 4. Deposition rate *vs.* square root of H_2 partial pressure for W films deposited at 285°C from WF_6-H_2-Ar gas mixtures. Total pressure = 1.4 torr. (1 torr = 133 Pa.) Curve C1 results from experiments performed with a clean quartz ware; curve Di is obtained from experiments carried out with a W deposit on the quartz ware. The meanings of symbols used for data points are given in Table II.

boat in proximity to the test wafer positions. Under these conditions, the surface area of W deposition can be estimated at several hundred cm². The rate constant calculated from the slope of the straight line (Di) is 5.47 nm-min^{-1}-torr$^{-1/2}$. In other words, when a W deposit appears and can be detected on the quartz ware, the growth rate of metal on the test wafers is reduced by 32% whatever the number of selective deposition runs already performed. Nevertheless, the reaction order with respect to hydrogen remains equal to one-half.

The deposition rate of W films prepared from WF_6-H_2 gas mixture has been determined as a function of H_2 partial pressure (Fig. 5). Curve (C1) shown in Fig. 5 represents the kinetic data obtained for deposition experiments carried out with WF_6-H_2-Ar mixtures (Fig. 4). The WF_6 partial pressure was relatively low (3-8 mtorr). Two kinetic regimes can be distinguished. First, under hydrogen partial pressures higher than 0.7 torr, the deposition rate of W films is quite similar to that obtained with argon in the gas phase. Thus, the growth rate displays no

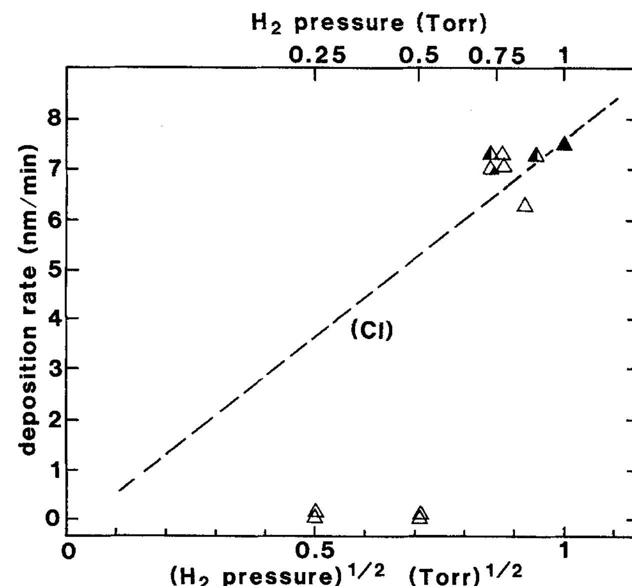

Fig. 5. Deposition rate *vs.* square root of H_2 partial pressure for films deposited at 285°C from WF_6-H_2 mixtures. (1 torr = 133 Pa.) WF_6 partial pressure = (3-8) mtorr. Curve C1 (dashed line) reports the data given in Fig. 4. The meanings of symbols used for data points are given in Table II.

Downloaded on 2015-03-18 to IP 152.14.136.77 address. Redistribution subject to ECS terms of use (see ecsdl.org/site/terms_use) unless CC License in place (see abstract).

dependence on changes in the argon partial pressure. Second, when the hydrogen partial pressure is less than 0.6 torr, the thickness of W films is limited to 15 nm, *i.e.*, the metal can be deposited only via the Si reduction of WF_6 occurring during the first step and the growth rate of W films via the H_2 reduction of WF_6 is about zero.

Selectivity.—The Si reduction of WF_6 yields perfect selectivity since no reaction can take place on SiO_2.

The symbols in Fig. 3-5 show the selective nature of deposition via the H_2 reduction of WF_6 as a function of WF_6 and H_2 partial pressures. Selectivity dependence on gas partial pressures is valid only for a deposition time of 15 min. For longer deposition times or thicker W films, selectivity would in all likelihood be lost owing to the development of W nuclei on the SiO_2 surface.

Selectivity deteriorates with increasing WF_6 partial pressure (Fig. 3). Under a hydrogen partial pressure of 0.44 torr, deposition remains selective at WF_6 partial pressures of less than 15 mtorr and W films will grow at a rate of only 15 nm/min. Selectivity is preserved at higher deposition rates: under an H_2 partial pressure of 0.75 torr with or without argon in the gas phase, 120 nm thick selective W films have been routinely deposited.

The correlation between selectivity and hydrogen partial pressure is shown in Fig. 4. Failure of selectivity occurs more frequently with increasing hydrogen partial pressure. For a given H_2 partial pressure (0.5 torr, for example), selectivity depends only on WF_6 partial pressure, *i.e.*, a failure of selectivity is observed under a WF_6 partial pressure higher than 15 mtorr. When a W deposit appears on the quartz boat, not only does the deposition rate fall off rapidly, but selectivity is more often lost. Consequently, after ten or 15 deposition runs, the quartz boat and reactor were cleaned in HF-HNO_3 solution to etch an eventual W deposit and oxidized dummy wafers were renewed.

Discussion

Reaction mechanism.—The kinetics of the chemical vapor deposition of W films via the H_2 reduction of WF_6 have been already extensively studied and Bryant (6) has analyzed experimental rate data. The reaction mechanism comprises five main sequences: (*i*) diffusion of reactants to the surface, (*ii*) adsorption of reactants on the surface, (*iii*) reaction in the adsorbed phase on the surface, (*iv*) desorption of gas products, and (*v*) diffusion of gas products from the surface.

At high substrate temperatures ($T > 700°C$), relatively low reactant flow rates, and high total pressure, the mass transport process by diffusion in the gas phase is the rate-controlling step (12). Throughout the temperature and pressure ranges investigated for selective tungsten deposition, the kinetic data may be interpreted on the basis of the Langmuir-Hinshelwood model which is currently used in heterogeneous catalysis. In previous studies (5-7), the dissociative adsorption of hydrogen on tungsten was considered as the rate-limiting step. This assumption does not account for the large decrease in deposition rate observed when W deposits on the quartz ware. Nor can this decrease in deposition rate be explained by a depletion of reactant gases due to the large increase in deposition area. Indeed, hydrogen consumption is only 0.4 cm^3/min when 60 cm^2 of metal are deposited at a rate of 10 nm/min. In the reaction scheme proposed in the present work (see Appendix), HF has been considered to affect the surface reaction rate in the adsorbed phase. Details of the procedure used to establish the expression of growth rate of the W films are given in the Appendix.

The actual HF partial pressure, P_C, in the reactor is proportional to the growth rate of tungsten, *i.e.*, to the square root of hydrogen pressure, $(P_B)^{1/2}$, and to the surface area of W deposition; therefore

$$P_C = \beta(a_o + a_1)(P_B)^{1/2} \quad [1]$$

where a_o is the surface area for selective deposition and a_1 is the surface area of deposition when a W deposit is detected on the quartz ware, $a_1 >> a_o$.

Using the value of HF partial pressure given by Eq. [1], the expression [A-15] for the growth rate becomes

$$G_R = [k_R\alpha(1 - \epsilon)N_s\epsilon K_B - k'_R N_s^2\epsilon^2 K_C\beta(a_o + a_1)](P_B)^{1/2} \quad [2]$$

Therefore, the reaction orders with respect to WF_6 and H_2 (zero and one-half, respectively) provided by Eq. [2] are in good agreement with the experimental values determined during this study as well as with the findings of other investigators (5-7). By plotting G_R *vs.* $(P_B)^{1/2}$, two curves can be obtained. When the quartz ware is clean, the surface area, a_1, is zero and the slope of the straight line (C1) is given by

$$S_{(C1)} = k_R\alpha(1 - \epsilon)N_s\epsilon K_B - k'_R N_s^2\epsilon^2 K_C\beta a_o \quad [3]$$

After several runs, when the metal is deposited on the quartz tube, boat, and dummy wafers, the deposition rate decreases and the slope of the straight line (Di) is given by

$$S_{(Di)} = S_{(C1)} - k'_R N_s^2\epsilon^2 K_C\beta a_1 \quad [4]$$

Thus, the experimental results as given in Fig. 3 and 4 can be described by Eq. [2].

The effect of HF partial pressure on the H_2 reduction of WF_6 has been studied in the past. Berkeley *et al.* (13) have shown that a concentration of HF equal to about 25% of the volume of reactants was sufficient to inhibit the deposition of tungsten from static reacting gases. On the contrary, according to Cheung (5), the addition of up to 40% HF to the WF_6-H_2 gas flow system did not have more than a dilution effect on the deposition rate. This apparent discrepancy can be explained on the basis of the mechanism proposed (see Appendix) according to which a blocking effect of HF on the deposition process occurs in step [R]. Under relatively high WF_6 partial pressures, such as those used by Cheung, the value for ϵ^2 will be very small. Therefore, Eq. [A-15] can be simplified by neglecting the second term in the right member, which gives

$$G_R = k_R\alpha(1 - \epsilon)N_s\epsilon K_B(P_B)^{1/2} \quad [5]$$

And by neglecting ϵ with respect to unity, the expression becomes

$$G_R = k_R N_s\epsilon K_B\alpha(P_B)^{1/2} \quad [6]$$

Thus, it can be established that the growth rate of W films is independent of HF partial pressure but only under HF pressures higher by a factor of 100-1000 than those used in the present study.

Under hydrogen partial pressures of less than 0.6 torr, the growth rate of W films produced in WF_6-H_2 gas systems has been found dependent on the orientation of the wafer surface with respect to the gas flow. With the wafer surface parallel to the gas flow, the growth rate is zero (Fig. 5). On the other hand, with the wafer surface perpendicular to the gas flow and under analogous reactant partial pressures, W films were deposited (7, 8). The deposition rate dependence on wafer surface orientation may be linked to the hydrodynamics of the gas system. This point remains the focus of continuing studies.

Selectivity.—The processing conditions leading to the loss of selectivity given in Fig. 3-5 are in good agreement with those put forward by Saraswat *et al.* (8). Losses in selectivity can be linked to an increase in HF partial pressure in the reactor. The selective nature of the W deposition process deteriorates when the growth rate (or HF pressure) is increased and also specially at the edges of the large deposition zones, *i.e.*, in the areas of highest HF pressure. As has already been reported by Cuomo (14), the glass substrate is etched around the W deposition zone by HF liberated from the reduction reaction. In this ablative zone, water vapor is formed on the SiO_2 surface and WF_6 can be hydrolyzed to form tungsten oxyfluoride, WOF_4. A tungsten compound containing fluorine atoms has been detected by x-ray probe analysis around the ablative zone on the glass substrate (14). At low temperature

Downloaded on 2015-03-18 to IP 152.14.136.77 address. Redistribution subject to ECS terms of use (see ecsdl.org/site/terms_use) unless CC License in place (see abstract).

(285°C), the etching of SiO_2 due to HF formed by the H_2 reduction of WF_6 is very slight. Nevertheless, water vapor is probably formed on the SiO_2 surface and WF_6 may be locally converted into tungsten oxyfluoride. This compound serves as a nucleating site for W deposition. Hydrolysis is favored under relatively high WF_6 partial pressure and selectivity is reduced with increasing WF_6 pressure (Fig. 3). The nuclei grow slowly during the first minutes of the deposition process; their development thereafter accelerates, and, for longer periods, the selective nature of the deposition process becomes entirely lost.

The advantage of deposition with the wafer surface parallel to the gas flow is a shortening of the HF residence time on the SiO_2 surface. This ought to improve selectivity with respect to wafers placed perpendicular to the gas flow. This point, however, remains to be ascertained by comparative experiments. A parallel configuration implies a higher total pressure than if the wafers are perpendicular to the gas flow. This increase in total pressure has been achieved in the present study by adding argon to the gas system.

Selectivity of W deposition can be further improved by various other means: both deposition area and W growth rate must be as small as possible; a low deposition temperature minimizes the interaction between HF and SiO_2.

Conclusion

The kinetic data for selective tungsten deposition via the H_2 reduction of WF_6 can be interpreted on the basis of the Langmuir-Hinshelwood model. The surface reaction between fluorine and hydrogen atoms in the adsorbed phase is considered as the rate-controlling step. The deposition rate is dependent on the HF partial pressure and, consequently, on the surface area of W deposition. To minimize this surface area and obtain a good reproducibility on the deposition rate, the quartz tube, boat, and oxidized dummy wafers have to be free of any W deposit. The selectivity of the deposition process deteriorates with increasing WF_6 partial pressure and deposition rate. The loss of selectivity seems to be linked to an increase in HF partial pressure in the reactor. The selective nature of the process can certainly be preserved under processing conditions in which HF partial pressure in the reactor and the interaction between HF and SiO_2 are minimized.

Manuscript submitted April 9, 1985; revised manuscript received July 12, 1985.

Centre National d'Etudes des Télécommunications assisted in meeting the publication costs of this article.

APPENDIX

The different steps of the reaction mechanism for the H_2 reduction of WF_6 can be schematically represented as follows.

1. Adsorption of WF_6

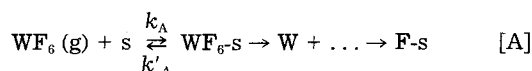

$$WF_6\,(g) + s \underset{k'_A}{\overset{k_A}{\rightleftarrows}} WF_6\text{-}s \rightarrow W + \ldots \rightarrow F\text{-}s \qquad [A]$$

2. Dissociative adsorption of hydrogen

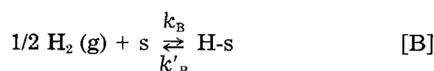

$$1/2\ H_2\,(g) + s \underset{k'_B}{\overset{k_B}{\rightleftarrows}} H\text{-}s \qquad [B]$$

3. Surface reaction in the adsorbed phase

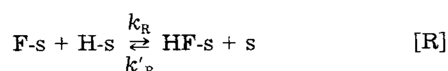

$$F\text{-}s + H\text{-}s \underset{k'_R}{\overset{k_R}{\rightleftarrows}} HF\text{-}s + s \qquad [R]$$

4. Desorption of HF

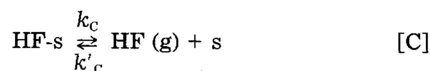

$$HF\text{-}s \underset{k'_C}{\overset{k_C}{\rightleftarrows}} HF\,(g) + s \qquad [C]$$

where k and k' are the rate constants of the direct and reverse reactions, respectively. K is the equilibrium constant with $K = k/k'$.

The Langmuir-Hinshelwood model is based on three main assumptions. First, the adsorption sites, s, on the surface of tungsten are equivalent and the adsorption of different gases (WF_6, H_2, and HF) is a competitive process. Second, the rate-limiting step is the surface reaction in the adsorbed phase; thus, the other surface processes are in equilibrium. Moreover, the surface reaction is assumed to be an opposing reaction, *i.e.*, the adsorbed species, F-s and H-s, can be formed by the adsorption of HF vapor on the tungsten surface. Nevertheless, the overall reduction reaction is not a reverse process. Third, the rate of the surface reaction, [R], is proportional to the concentrations of adsorbed species.

In order to establish an expression describing the growth rate of W films from WF_6-H_2 systems, some additional assumptions have been considered. The adsorption of WF_6 on tungsten produces fluorine atoms, called F-s in reaction [A], which are strongly adsorbed on the surface, *i.e.*, the equilibrium constant, K_A, in process [A] is very high. Some support for this assumption is provided by experimental data on the interactions between tungsten and WF_6 molecules or fluorine atoms (15-17). However, neither the stages from adsorbed fluorine atoms to WF_5 or WF_6 gas molecules nor the steps in the reverse processes have been completely understood. Finally, hydrogen and HF are assumed to be weakly adsorbed on tungsten, *i.e.*, the equilibrium constants, K_B and K_C, are very low.

To simplify the formalism of the rate equations, the subscripts A, B, and C will be used to designate the gases WF_6, H_2, and HF, respectively.

Let N_s be the total number of surface sites per square centimeter and let Θ_s, Θ_A, Θ_B, and Θ_C be the fractions of the surface sites which are free and covered by A, B, and C, respectively. In other words, Θ_s, Θ_A, Θ_B, and Θ_C are the mole fractions of free sites and adsorbed species, WF_6-s, H-s, and HF-s, *i.e.*, $\Theta_s = 1 - \Theta_A - \Theta_B - \Theta_C$. The concentrations of the adsorbed species and free sites on the W surface are given by

$$|WF_6\text{-}s| = N_s\Theta_A \qquad [A\text{-}1]$$

$$|H\text{-}s| = N_s\Theta_B \qquad [A\text{-}2]$$

$$|HF\text{-}s| = N_s\Theta_C \qquad [A\text{-}3]$$

$$|s| = N_s\Theta_s \qquad [A\text{-}4]$$

Since the adsorption step [A] is in equilibrium, the fraction of the surface sites occupied by WF_6 molecules can be expressed as a function of gas pressures (P_A, P_B, and P_C) using the steady-state equation (18)

$$\Theta_A = \frac{K_AP_A}{1 + K_AP_A + K_B(P_B)^{1/2} + K_CP_C} \qquad [A\text{-}5]$$

where K_A, K_B, and K_C are the equilibrium constants of the processes [A], [B], and [C], respectively.

Since H_2 and HF are weakly adsorbed and WF_6 strongly adsorbed on the W surface, the equilibrium constants K_B and K_C are very small and can be neglected with respect to K_A. Equation [A-5] can be simplified, and the term Θ_A is almost equal to unity. Setting

$$\epsilon = 1 - \Theta_A \qquad [A\text{-}6]$$

the value of ϵ will be very small.

The concentration of adsorbed fluorine atoms is assumed to be proportional to Θ_A and can be expressed by the following equation

$$|F\text{-}s| = \alpha(1 - \epsilon) \qquad [A\text{-}7]$$

Consequently, the concentration of fluorine atoms adsorbed on the W surface is independent of gas pressures. The terms Θ_B and Θ_C can be calculated in the same way as Θ_A (18). Since the sum $[K_B(P_B)^{1/2} + K_CP_C]$ is negligible with respect to unity, the simplified expressions of Θ_B, Θ_C, and Θ_s are the following

$$\Theta_B = \epsilon K_B(P_B)^{1/2} \qquad [A\text{-}8]$$

$$\Theta_C = \epsilon K_CP_C \qquad [A\text{-}9]$$

$$\Theta_s = \epsilon \qquad [A\text{-}10]$$

Furthermore, the concentrations of the adsorbed species and free sites on the W surface become

$$|H\text{-}s| = N_s\epsilon K_B(P_B)^{1/2} \qquad [A\text{-}11]$$

Downloaded on 2015-03-18 to IP 152.14.136.77 address. Redistribution subject to ECS terms of use (see ecsdl.org/site/terms_use) unless CC License in place (see abstract).

$$|\text{HF-s}| = N_s \epsilon K_C P_C \quad [A\text{-}12]$$

$$|\text{s}| = N_s \epsilon \quad [A\text{-}13]$$

The growth rate of W films, G_R, is equal to the rate of the surface reaction [R] which is considered to be the rate-limiting process. This surface reaction is an opposing reaction, and its rate is given by

$$G_R = k_R|\text{F-s}||\text{H-s}| - k'_R|\text{HF-s}||\text{s}| \quad [A\text{-}14]$$

Using Eq. [A-7] and Eq. [A-11]-[A-13], this rate equation takes the form

$$G_R = k_R\alpha(1 - \epsilon)N_s\epsilon K_B(P_B)^{1/2} - k'_R N_s^2 \epsilon^2 K_C P_C \quad [A\text{-}15]$$

REFERENCES

1. J. M. Shaw and J. A. Amick, *RCA Rev.*, **31**, 306 (1970).
2. Y. Pauleau, *Thin Solid Films*, **122**, 243 (1984).
3. N. E. Miller and I. Beinglass, *Solid State Technol.*, **23**, 79 (1980).
4. N. E. Miller and I. Beinglass, *ibid.*, **25**, 85 (1982).
5. H. Cheung, in "Proceedings of the Third International Conference on Chemical Vapor Deposition," F. A. Glaski, Editor, p. 136, The American Nuclear Society, Hinsdale, IL (1972).
6. W. A. Bryant, *This Journal*, **125**, 1534 (1978).
7. E. K. Broadbent and C. L. Ramiller, *ibid.*, **131**, 1427 (1984).
8. K. C. Saraswat, S. Swirhun, and J. P. McVittie, in "VLSI Science and Technology/1984," K. E. Bean and G. A. Rozgonyi, Editors, p. 409, The Electrochemical Society Softbound Proceeding Series, Pennington, NJ (1984).
9. K. Y. Tsao and H. H. Busta, *This Journal*, **131**, 2702 (1984).
10. T. Moriya, K. Yamada, Y. Tsunashima, S. Nakata, and M. Kashiwagi, Extended Abstracts of the 15th Conference on Solid State Devices and Materials, p. 225, Tokyo (1983).
11. Y. Pauleau, *Bull. Soc. Chim. France*, **4**, 583 (1985).
12. W. R. Holman and F. J. Huegel, *J. Vac. Sci. Technol.*, **11**, 701 (1974).
13. J. F. Berkeley, A. Brenner, and W. E. Reid, Jr., *This Journal*, **114**, 561 (1967).
14. J. J. Cuomo, in "Proceedings of The Third International Conference on Chemical Vapor Deposition," F. A. Glaski, Editor, p. 270, The American Nuclear Society, Hinsdale, IL (1972).
15. L. V. McCarty, W. E. Reith, and M. T. Simon, *This Journal*, **121**, 1372 (1974).
16. J. L. Philippart, J. Y. Caradec, B. Weber, and A. Cassuto, *ibid.*, **125**, 162 (1978).
17. M. Metlay and G. E. Kimball, *J. Chem. Phys.*, **16**, 779 (1948).
18. G. W. Castellan, "Physical Chemistry," 2nd ed., p. 795, Addison-Wesley, New York (1971).

A Diffusion Model for Electron-Hole Recombination in Zn_2SiO_4:(Mn,As) Phosphors

D. J. Robbins,*[,1] N. S. Caswell,* Ph. Avouris, E. A. Giess,* I. F. Chang,* and D. B. Dove

IBM Thomas J. Watson Research Center, Yorktown Heights, New York 10598

ABSTRACT

Optical techniques have been used to study the extended persistence of luminescence in willemite phosphors coactivated with Mn and As. Absorption and photoluminescence excitation spectroscopy establish that the Mn_{Zn}^{2+} impurity ground state lies 3.9 ± 0.1 eV below the conduction bandedge in willemite. Laser pulse excitation at energies > 3.9 eV has been used to generate Mn_{Zn}^{2+} luminescence decay curves. At short times ($t < 100$ ms), the shape of these decay curves depends strongly on both temperature and As concentration in the samples (N_{As}). These pulse response curves have been analyzed using a bimolecular kinetic model. The behavior of the model parameters as a function of N_{As} is interpreted in terms of a diffusion-controlled recombination between trapped electrons and ionized Mn centers. When $N_{As} < 1 \times 10^{19}$ cm^{-3}, the recombination is dominated by thermal emission of electrons to the conduction band. When $N_{As} > 2 \times 10^{19}$ cm^{-3}, diffusion by intertrap tunneling is dominant.

Manganese-activated willemite (Zn_2SiO_4:Mn), when coactivated with As, forms the phosphor system designated P39 (1). The active luminescence is the $^4T_1 \rightarrow {}^6A_1$ intracenter d electron relaxation of the Mn_{Zn}^{2+} impurity with lifetime $\tau_e \sim 10$ msec (2). The addition of As introduces a long nonexponential afterglow to the decay. This extended persistence of the P39 phosphor system makes it of considerable current interest as an antiflicker phosphor in displays where the refresh rate must be minimized, such as computer data display.

The Zn_2SiO_4:(Mn,As) phosphor was originally reported by Frohlich and Fonda (3). They investigated a number of approaches to increasing the persistence of Mn_{Zn}^{2+} luminescence in willemite, including quenching from high temperature, variation of stoichiometry, and incorporation of many coactivator impurities. Of these, the addition of As impurity to Zn_2SiO_4:Mn was found to be most effective in extending persistence. Improved methods of synthesizing the coactivated phosphor have recently been reported (4). In addition, the effects of $AlPO_4$ substitution in the willemite lattice have been investigated (5), although it is not yet clear that significant improvements in brightness and persistence can be achieved in this way (6). There has been considerable effort devoted to studying the physics of the phosphorescence process in Zn_2SiO_4:(Mn,As). Most of these studies have involved measurement of thermal glow curves (7-14). More recently, photostimulated luminescence and conductivity measurements have been carried out (15-18). However, as yet, there is no general agreement about the recombination mechanism in this phosphor.

It is known empirically that for maximum enhancement of persistence in P39 phosphor the concentrations of Mn and As must be controlled within definite limits. State of-the-art antiflicker performance is achieved when Mn is ~0.1%, substituted for Zn, and the As concentration is somewhat lower. The Mn concentration is about ten times lower than that used in the Zn_2SiO_4:Mn (P1) phosphor system which does not exhibit extended persistence, so that the overall efficiency of the P39 phosphor is reduced. However, there is no quantitative model which can be used to assess whether the presently favored composition of P39 is indeed optimal, or to guide the development of new phosphor systems.

In order to improve our understanding of the mechanism of this phosphor's operation, it is necessary to have more quantitative information about the impurity energy levels in the bandgap of the willemite lattice, about the partitioning of excitation energy between electron traps

*Electrochemical Society Active Member.
[1]On leave from Royal Signals and Radar Establishment, Malvern, England WR14 3PS.

Downloaded on 2015-03-18 to IP 152.14.136.77 address. Redistribution subject to ECS terms of use (see ecsdl.org/site/terms_use) unless CC License in place (see abstract).